SIAM J. APPL. MATH.
Vol. 70, No. 6, pp. 1953–1976

CELLULAR IMMUNOTHERAPY FOR HIGH GRADE GLIOMAS: MATHEMATICAL ANALYSIS DERIVING EFFICACIOUS INFUSION RATES BASED ON PATIENT REQUIREMENTS*

YURI KOGAN†, URSZULA FORYŚ‡, OFIR SHUKRON†, NATALIE KRONIK†, AND ZVIA AGUR†

Abstract. To date, no effective cure has been found for high grade malignant glioma (HGG), current median survival for HGG patients under treatment ranging from 18 months (grade IV) to 5 years (grade III). Recently, T cell therapy for HGG has been suggested as a promising avenue for treating such resistant tumors, but clinical outcome has not been conclusive. For studying this new therapy option, a mathematical model for tumor–T cell interactions was developed, where tumor immune response was modeled by six coupled ordinary differential equations describing tumor cells, T cells, and their respective secreted cytokines and immune mediating receptors. Here we mathematically analyze the model in an untreated case and under T cell immunotherapy. For both settings we classify steady states, determine stability properties, and explore the global behavior of the model. Analysis suggests that in untreated patients, the system always converges to a steady state of a large tumor mass. An increase in the patient's pro-inflammatory activity only marginally reduces tumor load at steady state. This result suggests that the patient's own immune system is never sufficient for eliminating HGG. In contrast, infusion of T cells above a certain level, $S_{\min}$, renders a curative tumor-free steady state locally asymptotically stable. When the infusion rate is increased above a higher threshold, $S_{\max}$, this steady state becomes globally stable, providing a cure from any initial state of the system. These thresholds, as well as the infusion time required for tumor elimination for different doses, are computed explicitly, and can be personalized using patient-specific parameters. Our results suggest that reduction of tumor load and even tumor elimination can be achieved, either by significantly encouraging the endogenous immune response or by T cell infusion. This work provides an insight and practical guidelines for improving the efficacy of brain cancer immunotherapy by T cell infusion, which should be further studied clinically.

Key words. glioblastoma, mathematical model, T cell, ordinary differential equation, local and global stability analysis, steady state

AMS subject classifications. 37N25, 34C60, 92B05, 92C50

DOI. 10.1137/08073740X

1. Introduction.

Immunotherapy is a rapidly developing approach in cancer treatment, based on the premise that the immune system can be strengthened to fight the cancer. Different immunotherapy strategies have been considered for aiding the immune system in efficient recognition and destruction of tumor cells. These include cytokine immunotherapy [5] and cellular immunotherapy [12, 19, 23]. The latter method suggests treatment by addition of immune cells (autologous or allogeneic) previously presented with tumor-related antigens, which will directly attack and destroy tumor cells. Various cellular immunotherapy protocols are currently being developed and undergoing trials in both animals and humans.

The complex tumor–immune system interactions and their control by immunotherapy involve negative and positive feedback and processes having different rates and

*Received by the editors October 7, 2008; accepted for publication (in revised form) November 30, 2009; published electronically February 26, 2010. This work was supported by EU Marie Curie grant MRTN-CT-2004-503661, by EU-NEST project contract 12930, and by the Chai Foundation.
http://www.siam.org/journals/siap/70-6/73740.html
†Institute for Medical BioMathematics, 10 Hate'ena St., P.O.B. 282, Bene-Ataroth, 60991, Israel (yuri@imbm.org, ofir@imbm.org, natalie@imbm.org, agur@imbm.org).
‡Institute of Applied Mathematics and Mechanics, Faculty of Mathematics, Informatics and Mechanics, University of Warsaw ul. Banacha 2, 02-097 Warszawa, Poland (urszula@mimuw.edu.pl).
This author's work was supported by Polish Ministry of Science, grant 1 P03A 028 30.

different time scales. This complexity does not allow intuitive prediction of the effects of different factors on the final result, whereas mathematical models enable one to predict nonlinear complex dynamics. Previous studies [2, 3, 4, 6, 7, 14, 21, 24] put forward theoretical models of cancer immunology and immunotherapy. In particular, in [21], the ordinary differential equations (ODEs) system that describes the interaction between the tumor and immune cell is investigated, while in [14], a similar model considers also the effects of pro-immune cytokine interleukin-2 and the application of cellular and cytokine immunotherapy. In [6] the interaction between the tumor and natural killer cells and $CD8^+$ cells is investigated, including the effect of immunotherapy and sensitivity analysis. Further, the effects of chemotherapy together with vaccination are considered in [7]. Mathematical models for immunotherapy by IL-21 are validated in cancer-bearing animals [3] and optimal IL-21 therapy has been suggested [4].

In this work we focus on cellular immunotherapy of brain tumors using alloreactive or allogeneic cytotoxic T lymphocytes (CTLs), currently under clinical trials in high grade gliomas (HGGs), which are among the most aggressive and deadly brain tumors. HGGs include such tumor types as anaplastic astrocytoma, anaplastic oligodendroglioma (grade III HGG), and glioblastoma multiforme (GBM) (grade IV). These HGGs vary in life expectancy, but even with the best-known contemporary care survival does not exceed 1.5 years for GBM and 5 years for the less aggressive forms [15]. A novel cellular immunotherapy using alloreactive CTLs has been suggested [19, 20]. The clinical trials showed considerably prolonged survival in some cases in grade III HGG, but were unsuccessful in GBM patients.

A mathematical model for the application of cellular immunotherapy for HGG was proposed in [17]. It describes the interactions between the tumor and the immune system in the brain by a set of six ODEs, representing the dynamics of tumor cells, CTLs, transforming growth factor-beta (TGF-β), interferon-gamma (IFN-γ), and the mediating molecules major histocompatibility complex class I (MHCI) and major histocompatibility complex class II (MHCII). These six major role players are connected in a web of positive and negative feedback (for details see Figure 1 in [17]). In brief, a tumor located in the brain is rather sheltered from the immune system. Only activated CTL recruited from the peripheral blood can cross the blood brain barrier (BBB) to lyse tumor cells; activation of a CTL is enabled only if a T helper cell managed earlier to cross the BBB and to encounter a tumor-associated antigen on the surface of an antigen presenting cell displayed on an MHCII receptor. An activated CTL in the brain is able to identify and destroy a tumor cell by recognizing a tumor antigen presented on MHCI receptors on the tumor surface. To add to this complexity, tumor cells secrete an anti-inflammatory cytokine TGF-β, which reduces the efficacy of tumor cell lysis by a CTL. TGF-β also makes the BBB less permeable to activated CTLs. On the other hand, activated CTLs secrete IFN-γ, which induces MHCI and MHCII expression on the surface of tumor cells and antigen-presenting cells. In [17] it was shown that HGG grade III and grade IV can be represented by assigning proper values to the parameter representing maximal tumor growth rate. The model successfully retrieved the results of the clinical trial by Kruse et al. [19, 20], which used donor CTL infusions for brain tumor patients. This model varies from the models studied in the aforementioned studies, by considering the mediator role of MHC receptors and by focusing on the specific type of brain tumors.

In the present work, we explore the scope of behavior of the same model, with or without treatment, where treatment consists of constant infusion of exogenous CTLs, either alloreactive or allogeneic. For each setting, we study the steady states of the model and their stability, allowing classification of possible steady states of the

tumor under the influence of the immune system and treatment. This is one of the first theoretical works, establishing the mathematical basis for the administration of a novel adoptive cellular immunotherapy for HGG. The model is used for predicting clinical amounts of CTLs to be infused directly to the resection cavity in the brain in order to eradicate HGG.

Section 2 presents the generalized model and its basic properties. In section 3 we study the steady states of the untreated system. Section 4 is devoted to exploring the steady states of the system with treatment by a constant infusion of CTLs. Section 5 complements the results of sections 3 and 4, using explicit calculations and numerical solutions. Embedding the realistic parameters in the model, we estimate threshold values for successful treatment and time to tumor elimination.

2. The model and its basic properties. In this section we present the model equations and basic assumptions. We deduce existence, uniqueness, and boundedness of solutions, as well as existence of a compact global attractor. These results show that the system has a biologically reasonable behavior; i.e., cytokine levels, as well as receptor and cell numbers, do not drop below zero or diverge. They also suggest certain regularity is to be expected in the system behavior, though they do not rule out instability or chaos.

In [17], a system of six ODEs was used to describe the dynamics of tumor cell number, T, CTL number, C, quantities of TGF-β and INF-γ in the central spinal fluid (CSF), F_β and F_γ, respectively, and numbers of molecules of MHC class I and MHC class II per cell, MI and MII, respectively. In the present work, we simplify the notation used in [17] and further introduce a minor modification, as follows. MHC class I and MHC class II molecule numbers per cell are denoted by u and v, respectively. Instead of quantities of TGF-β and IFN-γ in the CSF we consider their concentrations in the CSF, denoted by x and y, respectively. The relations between quantity and concentration are given by $x = \frac{F_\beta}{V}$ and $y = \frac{F_\gamma}{V}$, where V is the volume of the CSF, assumed to be constant. This change requires the straightforward adjustment of parameter values used in [17], which is explained in Appendix. In the first stage of the analysis we also generalize the expressions used in [17], presenting the functions in generic form and specifying their important properties. Thus, the system of equations from [17] becomes

$$\begin{aligned}
\dot{T} &= r(T)T - f_T(x)g_T(u)h(T)CT,\\
\dot{C} &= f_C(T\cdot v)g_C(x) - \mu_C C + S(t),\\
\dot{x} &= f_x(T) - \mu_x x,\\
\dot{y} &= f_y(C) - \mu_y y,\\
\dot{u} &= f_u(y) - \mu_u u,\\
\dot{v} &= f_v(x)g_v(y) - \mu_v v,
\end{aligned} \tag{2.1}$$

where

- $r(T)$ is the rate of tumor growth;
- the function $f_T(x)$ represents the reduction of CTLs efficacy as a result of TGF-β;
- the function $g_T(u)$ describes the dependence of CTLs efficacy on the number of MHC class I receptors presented by a tumor cell;
- $h(T)$ is the function representing the effect of tumor mass on the tumor cell accessibility to CTLs;
- $f_C(T\cdot v)$ is the natural CTL recruitment function;

- $S(t)$ is the treatment function describing the momentary infusion rate of CTLs;
- μ_C is the CTLs death rate in the brain;
- $f_x(T)$ and $f_y(C)$ are the production functions of TGF-β and IFN-γ, by tumor cells and CTLs, respectively;
- μ_x and μ_y are the TGF-β and IFN-γ elimination rates, respectively;
- $f_u(y)$ is the MHC class I production function dependent on IFN-γ level;
- $g_v(y)$ and $f_v(x)$ are the MHC class II production due to IFN-γ and inhibition by TGF-β, respectively;
- μ_u and μ_v are the MHC class I and MHC class II elimination rates, respectively.

The model construction and the form of the equations are elaborated in [17]. Note that for all components of the system, except for T, we assume first-order elimination. In addition, we preserve here the distinction made in [17] between grade III and grade IV HGG by the values of $r(T)$.

We make the following biologically reasonable assumptions in order to determine the properties of the system (2.1):

- The functions r, f_T, g_T, h_T, f_C, g_C, S, f_x, f_y, f_u, f_v, and g_v are of class C^1 and have nonnegative values.
- $r(T)$ is decreasing on $[0, K]$, $r(0) = r_0 > 0$, and $r(K) = 0$, where K is the carrying capacity of the tumor. We also assume that for $0 \le T \le K$, $r''(T) \ge 0$.
- TGF-β decreases the efficacy of tumor killing by CTLs, up to some saturation limit; i.e., $f_T(x)$ is decreasing, $f_T(0) = 1$, $\lim_{x\to+\infty} f_T(x) = a_{T,x} > 0$, and f'_T is increasing.
- MHC class I receptors are necessary for CTLs action, and they increase CTL efficacy up to some saturation limit; i.e., $g_T(0) = 0$, $\lim_{u\to+\infty} g_T(u) = a_T > 0$, $g_T(u)$ is increasing, and g'_T is decreasing.
- A large tumor mass hampers CTL access to tumor cells and, therefore, reduces the kill rate; i.e., $h_T(T)$ is decreasing, $h_T(0) = 1$, $\lim_{T\to+\infty} h_T(T) = 0$, and h'_T is increasing. Note that although this factor can annulate the efficacy of CTLs, this will never happen in cases of interest because $T \le K$.
- The total number of MHC class II receptors on all tumor cells determines the recruitment of CTLs. The rate of CTL entrance is limited; i.e., f_C is increasing from $f_C(0) = 0$ to $\lim_{Tv\to+\infty} f_C(Tv) = a_{C,v} > 0$, and f'_C is decreasing.
- TGF-β reduces recruitment of CTLs down to some minimal level; i.e., $g_C(0) = 1$, $\lim_{x\to+\infty} g_C(x) = a_{C,x} > 0$, $g_C(x)$ is decreasing, and g'_C is increasing.
- $S(t)$ is nonnegative and constant, representing the immunotherapy by infusion, which we assume to be constant. However, in further studies it can be replaced by a more complex function representing nonconstant treatment.
- TGF-β is secreted by all the tumor cells, and, in addition, there is a base level secretion of TGF-β; i.e., $f_x(0) = g_x$, $f_x(T)$ is increasing, $\lim_{T\to+\infty} f_x(T) = +\infty$, and f'_x is nonincreasing.
- IFN-γ is secreted by all the CTLs, its base level is negligible; i.e., $f_y(0) = 0$, $f_y(C)$ is increasing, $\lim_{C\to+\infty} f_y(C) = +\infty$, and f'_y is nonincreasing.
- There is a constant basic production of MHC class I receptors at the cell surface, while IFN-γ increases this production up to some level; i.e., $f_u(0) = g_u > 0$, $\lim_{y\to+\infty} f_u(y) = g_u + a_{u,y}$, $a_{u,y} > 0$, $f_u(y)$ is increasing, and f'_u is decreasing.

- TGF-β reduces MHC class II production down to some minimal level; i.e., $f_v(0) = 1$, $\lim_{x\to+\infty} f_v(x) = a_{v,x}$, $f_v(x)$ is decreasing, and f_v' is increasing.
- IFN-γ is necessary to induce production of MHC class II receptors and increases it up to some level; i.e., $g_v(0) = 0$, $\lim_{y\to+\infty} g_v(y) = a_{u,y} > 0$, $g_v(y)$ is increasing, and g_v' is decreasing.

These assumptions imply that all solutions to the system (2.1) are nonnegative for nonnegative initial conditions and they are defined for every $t \geq 0$. Further, these solutions have the following properties:

1. For the first equation it is obvious that $\dot{T} \leq r(T)T$. Therefore, if $T(0) \leq K$, then $T \leq K$, for $t \geq 0$.
2. The maximal value of the expression $f_C(Tv)g_C(x)$ is equal to $a_{C,v}$. Therefore, $\dot{C} \leq a_{C,v} + S_{\max} - \mu_C C$ which implies $C \leq C_{\max} = \max\{\frac{a_{C,v}+S_{\max}}{\mu_C}, C(0)\}$.
3. The first variable T is bounded by K and hence, $f_x(T) \leq f_x(K)$. As for the variable C, we obtain $x \leq x_{\max} = \max\{\frac{f_x(K)}{\mu_x}, x(0)\}$.
4. As above, $y \leq y_{\max} = \max\{\frac{f_y(C_{\max})}{\mu_y}, y(0)\}$.
5. Similarly, $u \leq u_{\max} = \max\{\frac{g_u+a_{u,y}}{\mu_u}, u(0)\}$.
6. The maximal value of $f_v g_v$ is equal to $a_{u,y}$ and hence, $v \leq v_{\max} = \max\{\frac{a_{u,y}}{\mu_v}, v(0)\}$.

Thus, we can state the following.

PROPOSITION 1. *All coordinates of the solution to the system* (2.1) *with nonnegative initial conditions are nonnegative and bounded.*

We are mainly interested in the asymptotic behavior of solutions to the system (2.1). We show now that the system has a compact global attractor. Although the system is highly nonlinear, we expect that the form of this attractor is simple. It is confirmed by numerical simulations we present in section 5 for the specific functions proposed in [17]. To show the existence of the attractor, we use the following notion of dissipativity (compare, e.g., [10]). Let $\dot{x} = F(x)$ be the system of equations defined on some Banach space X and $S_t(x_0)$, $x_0 \in X$, be the semigroup of solutions to this system. This semigroup (or the system, equivalently) is called dissipative, if there exists a bounded set $B \subset X$, which attracts all bounded sets from X. If X is finite-dimensional, then dissipativity yields existence of a global compact attractor.

PROPOSITION 2. *The system* (2.1) *has a compact global attractor in* $[0, K] \times (\mathbb{R}^+)^5$.

Proof. We show that the system (2.1) is dissipative. It is enough to find a function $W : X \to R$, where $X = [0, K] \times (\mathbb{R}^+)^5$ in our case, such that W is bounded on bounded sets, $\lim_{x\to\infty} W(x) = +\infty$, for every $x \in X$ the function $W(S_t(x))$ is differentiable, and $\nabla W \cdot F = \frac{d}{dt} W(S_t(x)) \leq \beta - \alpha W$ for some nonnegative constants α and β, where F denotes the right-hand side of the system (2.1). Let $W(T, C, x, y, u, v) = T + C + x + y + u + v$. Note that $r(T)T \in [0, r_0 K]$ on $[0, K]$ and therefore, $r(T)T \leq a - bT$, where $a = 2Kr_0$ and $b = r_0$. Hence,

$$\begin{aligned}\nabla W \cdot F = {} & r(T)T - f_T(x)g_T(u)CTh_T(T) + f_C(Tv)g_C(x) - \mu_C C + S + f_x(T) \\ & - \mu_x x + f_y(C) - \mu_y y + f_u(y) - \mu_u u + f_v(x)g_V(y) - \mu_v v \leq a - bT + a_{C,v} \\ & - \mu_C C + S_0 + \bar{f}_x - \mu_x x + \bar{f}_y - \mu_y y + \bar{f}_u - \mu_u u + \bar{f}_v - \mu_v v \leq \beta - \alpha W,\end{aligned}$$

where $\alpha = \min\{b, \mu_C, \mu_x, \mu_y, \mu_u, \mu_v\}$ and $\beta = a + a_{C,v} + S_0 + \bar{f}_x + \bar{f}_y + \bar{f}_u + \bar{f}_v$. Dissipativity yields existence of a global compact attractor for the system (2.1). ∎

3. Steady states of the untreated system. In this section we study the existence and stability of steady states for the untreated system (2.1), i.e., $S = 0$. We

show that the unique steady state defined by $T = 0$ and $C = 0$ always exists but is unstable. This steady state will be denoted "no disease, no immunity (NDNI) steady state." In addition, there always exists a steady state defined by $T = K$ and $C = 0$, which we will term "disease, no immunity (DNI) steady state." Its stability depends on the condition described in Proposition 3. This condition is, in fact, an inequality that demands that the degradation constants of the pro-immune components in the system (CTLs, IFN-γ, MHC class II) are large enough to ensure their quick removal from the tumor environment. Proposition 4 shows that the same inequality implies that there are no other steady states in the untreated case.

From the first equation of system (2.1), it is obvious that at steady state, either $T = 0$ or

$$r(T) = f_T(x)g_T(u)h_T(T)C \quad \text{for} \quad T \neq 0. \tag{3.1}$$

In the following subsections we show that the system (2.1) may have two or more steady states, depending on model parameters. For studying their stability we use the Jacobi matrix of the system (2.1):

(3.2)
$$\begin{pmatrix}
r'(T)T + r(T) & -f_T(x)g_T(u) & -f'_T(x)g_T(u) & 0 & -f_T(x)g'_T(u) & 0 \\
-f_T(x)g_T(u)C \cdot\big(h_T(T) + Th'_T(T)\big) & h_T(T)T & h_T(T)CT & & h_T(T)CT & \\
f'_C(Tv)g_C(x)v & -\mu_C & f_C(Tv)g'_C(x) & 0 & 0 & f'_C(Tv)g_C(x)T \\
f'_x(T) & 0 & -\mu_x & 0 & 0 & 0 \\
0 & f'_y(C) & 0 & -\mu_y & 0 & 0 \\
0 & 0 & 0 & f'_u(y) & -\mu_u & 0 \\
0 & 0 & f'_v(x)g_v(y) & f_v(x)g'_v(y) & 0 & -\mu_v
\end{pmatrix}.$$

3.1. NDNI steady state. When $T = 0$ at steady state, the steady state values for other variables can be computed as follows:

$$C = 0, \quad x = \frac{f_x(0)}{\mu_x} = \frac{g_x}{\mu_x} > 0, \quad y = \frac{f_y(0)}{\mu_y} = 0,$$
$$u = \frac{f_u(0)}{\mu_u} = \frac{g_u}{\mu_u} > 0, \quad v = \frac{f_v(x)g_v(0)}{\mu_v} = 0.$$

Therefore, there exists a unique NDNI steady state $(0, 0, \frac{g_x}{\mu_x}, 0, \frac{g_u}{\mu_u}, 0)$. For this steady state only one nonzero term exists in the first row of the Jacobi matrix (3.2). Hence, the first eigenvalue of the system, $\lambda_1 = r_0 > 0$, and this implies instability of this state. Moreover, it is easy to see that $\lambda_5 = -\mu_u$ and therefore, NDNI is a saddle point.

3.2. DNI steady state. Coming back to (3.1), we see that it is satisfied by $T = K$ and $C = 0$. From the second equation of system (2.1) under the condition $S \equiv 0$, there should be $f_C(Tv)g_C(x) = \mu_C C$ at any steady state. Using the assumptions $f_y(0) = 0$, $g_v(0) = 0$, and $f_C(0) = 0$, we see that $C = y = v = 0$. Hence, there is a DNI steady state $(K, 0, x_K, 0, u_K, 0)$, where $x_K = \frac{f_x(K)}{\mu_x}$ and $u_K = \frac{g_u}{\mu_u}$.

The Jacobi matrix in this case takes the following form:

(3.3)
$$\begin{pmatrix} r'(K)K & -f_T(x_K)g_T(u_K)h_T(K)K & 0 & 0 & 0 & 0 \\ 0 & -\mu_C & 0 & 0 & 0 & f'_C(0)g_C(x_K)K \\ f'_x(K) & 0 & -\mu_x & 0 & 0 & 0 \\ 0 & f'_y(0) & 0 & -\mu_y & 0 & 0 \\ 0 & 0 & 0 & f'_u(0) & -\mu_u & 0 \\ 0 & 0 & 0 & f_v(x_K)g'_v(0) & 0 & -\mu_v \end{pmatrix}.$$

Calculating the characteristic polynomial for the steady state above, one obtains

$$P(\lambda) = (\lambda - r'(K)K)(\lambda + \mu_x)(\lambda + \mu_u)[(\lambda + \mu_y)(\lambda + \mu_v)(\lambda + \mu_C) - A],$$

where

$$A = f'_y(0)f'_C(0)g_C(x_K)f_v(x_K)g'_v(0)K. \tag{3.4}$$

Since $r'(K)K$ is negative, while μ_x and μ_u are positive, the sufficent condition of stability of the DNI steady state is negativeness of the real parts of roots of the polynomial

$$Q(\lambda) = (\lambda + \mu_y)(\lambda + \mu_v)(\lambda + \mu_C) - A.$$

From the model assumptions it follows that $A \geq 0$. If $A = 0$, all three roots of Q are negative real. Upon increasing A, the maximal root increases, while the two other roots remain negative, or become complex with negative real part (since the sum of the three roots remains unchanged). Thus, for $A < \mu_y\mu_v\mu_C$ all three roots have negative real parts, while at $A = \mu_y\mu_v\mu_C$, the maximal root becomes 0 and the steady state loses its stability when $A > \mu_y\mu_v\mu_C$.

PROPOSITION 3. *If*

$$A < \mu_y\mu_v\mu_C, \tag{3.5}$$

where A is defined by (3.4)*, then the DNI steady state $(K, 0, x_K, 0, u_K, 0)$ is locally asymptotically stable (LAS). The inverse inequality implies instability of this state.*

3.3. Positive DI steady states. Let $(T_p, C_p, x_p, y_p, u_p, v_p)$ denote a steady state with $T_p > 0$, $C_p > 0$. Then

$$x_p = \frac{f_x(T_p)}{\mu_x}, \quad y_p = \frac{f_y(C_p)}{\mu_y}, \quad u_p = \frac{f_u(y_p)}{\mu_u}, \quad v_p = \frac{f_v(x_p)g_v(y_p)}{\mu_v}.$$

This means that if there exist $T_p > 0$ and $C_p > 0$, then the positive steady state is defined. We will term such a steady state "disease, immunity (DI) steady state." To find these steady states, we need to solve the system of two equations

$$r(T_p) = f_T\left(\frac{f_x(T_p)}{\mu_x}\right) g_T\left(\frac{f_u\left(\dfrac{f_y(C_p)}{\mu_y}\right)}{\mu_u}\right) h_T(T_p)C_p\,, \tag{3.6}$$

$$f_C\left(\frac{f_v\left(\dfrac{f_x(T_p)}{\mu_x}\right) g_v\left(\dfrac{f_y(C_p)}{\mu_y}\right) T_p}{\mu_v}\right) g_C\left(\frac{f_x(T_p)}{\mu_x}\right) = \mu_C C_p\,. \tag{3.7}$$

Consider (3.7) and define the auxiliary function

$$H_T(C) = f_C\left(\frac{f_v\left(\frac{f_x(T)}{\mu_x}\right) g_v\left(\frac{f_y(C)}{\mu_y}\right) T}{\mu_v}\right) g_C\left(\frac{f_x(T)}{\mu_x}\right) - \mu_C C$$

for $T \geq 0$. For every $T \geq 0$, $H_T(0) = 0$. Hence, if H_T is a strictly monotonic function, then there is no steady state with $C > 0$. Taking the derivative with respect to C one gets

$$\begin{aligned} H_T'(C) =& f_C'\left(\frac{f_v\left(\frac{f_x(T)}{\mu_x}\right) g_v\left(\frac{f_y(C)}{\mu_y}\right) T}{\mu_v}\right) \\ &\times \frac{f_v\left(\frac{f_x(T)}{\mu_x}\right) T}{\mu_v} g_v'\left(\frac{f_y(C)}{\mu_y}\right) \frac{f_y'(C)}{\mu_y} g_C\left(\frac{f_x(T)}{\mu_x}\right) - \mu_C. \end{aligned}$$

For a given T, if for all C there is $H_T'(C) < 0$, then no positive solution exists. Recall from the assumptions in section 2 the following properties: f_C', g_v', and f_y' are positive and nonincreasing, and f_C' and g_v' are decreasing. In addition, $\lim_{C\to\infty} f_y(C) = +\infty$. It follows that $H_T'(C)$ is decreasing; thus the condition $H_T'(0) < 0$ is sufficient to provide $H_T'(C) < 0$ for any C. On the other hand, if $H_T'(0) > 0$, we note that boundedness and monotonicity of g_v and g_v' imply that $g_v'(y) \to 0$ when $y \to +\infty$. This implies that for C big enough, $H_T'(C) < \epsilon - \mu_C$ with ϵ arbitrarily small; thus the equation $H_T(C) = 0$ has a positive solution. Moreover, $H_T'(C)$ is decreasing (the second derivative has a constant sign); thus there is only one positive C for which $H_T(C) = 0$. Note that this value of C may be larger than $C_{\max}$. In this case there still can be no positive steady state in the range of interest.

Further, using our assumptions we can obtain the following estimation for $0 \leq T \leq K$:

$$H_T'(0) < \frac{f_C'(0) f_v(x_K) K g_v'(0) f_y'(0) g_C(x_K)}{\mu_v \mu_y} - \mu_C,$$

where $x_K = \frac{f_x(K)}{\mu_x}$ is the x-coordinate of the DNI steady state.

PROPOSITION 4. *If $A < \mu_y\mu_v\mu_C$, that is,* (3.5) *is satisfied, then the untreated system has no steady state with $0 < T < K$.*

Propositions 3 and 4 suggest that for $A = \mu_y\mu_v\mu_C$ we can expect the appearance of a DI steady state and switch of stability between the DNI and DI steady states. We explore this issue numerically in section 5.

4. Steady states for the treated system. In this section we explore the steady states and their stability for system (2.1), with a positive, constant CTLs infusion rate, $S > 0$. We show that there exists the unique steady state defined by $T = 0$, $C = \frac{S}{\mu_C}$, and it is LAS for S large enough, as described by Proposition 5. We term it "no disease, immunity (NDI) steady state." Further analysis demonstrates the possibility of positive DI steady states.

4.1. NDI steady state and tumor elimination. For the system (2.1) with positive S, the steady state value of C is nonzero. The case $T_{st} = 0$ leads to

$$C_{st} = \frac{S}{\mu_C}, \quad x_{st} = \frac{f_x(0)}{\mu_x}, \quad y_{st} = \frac{f_y(C_{st})}{\mu_y}, \quad u_{st} = \frac{f_u(y_{st})}{\mu_u}, \quad v_{st} = \frac{f_v(x_{st})g_v(y_{st})}{\mu_v},$$

and all the coordinates, except for T_{st}, are positive. To examine the stability, we note that the Jacobi matrix for system (2.1) with positive constant S remains the same as in the untreated case. For the steady state $(0, C_{st}, x_{st}, y_{st}, u_{st}, v_{st})$ one gets the following matrix:

(4.1)
$$\begin{pmatrix} r_0 - g_T(u_{st})f_T(x_{st})C_{st} & 0 & 0 & 0 & 0 & 0 \\ f_C'(0)g_C(x_{st})v_{st} & -\mu_C & 0 & 0 & 0 & 0 \\ f_x'(0) & 0 & -\mu_x & 0 & 0 & 0 \\ 0 & f_y'(C_{st}) & 0 & -\mu_y & 0 & 0 \\ 0 & 0 & 0 & f_u'(y_{st}) & -\mu_u & 0 \\ 0 & 0 & f_v'(x_{st})g_v(y_{st}) & f_v(x_{st})g_v'(y_{st}) & 0 & -\mu_v \end{pmatrix}.$$

It is easy to see that the eigenvalues of the matrix (4.1) are equal to $-\mu_v$, $-\mu_u$, $-\mu_y$, $-\mu_x$, $-\mu_C$, and $r_0 - g_T(u_{st})f_T(x_{st})C_{st}$, the first five always being negative. For the last expression, we observe that r_0 and $f_T(x_{st})$ depend on parameter values, but not on S, while $g_T(u_{st})C_{st}$ is increasing (at least linearly) in S. Therefore, for S large enough, the last eigenvalue is also negative. Substituting the steady state values of the variables, we obtain the following condition.

PROPOSITION 5. *Let S be sufficiently large, so that*

$$\frac{S}{\mu_C} g_T\left(\frac{f_u\left(\frac{f_y(S/\mu_C)}{\mu_y}\right)}{\mu_u}\right) > \frac{r_0}{f_T\left(\frac{f_x(0)}{\mu_x}\right)}.$$

Then the NDI steady state $(0, C_{st}, x_{st}, y_{st}, u_{st}, v_{st})$ is LAS.

Proposition 5 provides a necessary condition for treatment to be efficacious in tumor elimination. Further, if S is large enough, we can obtain the global stability of this steady state. Indeed, let $S = S^*$, $C(t) > C^* = \frac{S^*}{\mu_C}(1-\epsilon)$ for ϵ arbitrarily small and t large enough. Consequently, if we put $y^* = \frac{f_y(C^*)}{\mu_y}(1-\epsilon_1)$ and $u^* = \frac{f_u(y^*)}{\mu_u}(1-\epsilon_2)$, for small ϵ_1, ϵ_2, then, starting from some moment, $u > u^*$ and therefore, $g_T(u)C > g_T(u^*)C^*$. Note also, that $g_T(u^*)C^*$ increases in S^* at least linearly. On the other hand, values of f_T and h_T are bounded from below: $h_T(T) \geq h_T(K)$ and $f_T(x) \geq f_T(x_{\max})$. Therefore, if we can supply the system with S^* large enough, such that $g_T(u^*)C^* > \frac{r_0}{h_T(K)f_T(x_{\max})}$, then $\dot{T} \leq -aT$, where $a = g_T(u^*)C^* - \frac{r_0}{h_T(K)f_T(x_{\max})} > 0$, and therefore, the tumor size decays to 0. Thus, we have the following remark.

Remark 1. If $\frac{S}{\mu_C} g_T(\frac{f_u(\frac{f_y(S/\mu_C)}{\mu_y})}{\mu_u}) > \frac{r_0}{f_T(\frac{f_x(K)}{\mu_x})h_T(K)}$, then the tumor size exponentially decays to 0.

Comparing to Proposition 5, the condition assumed in Remark 1 is stronger and requires larger values of the injection rate S.

4.2. Positive DI steady states. To find DI steady states $(T_p^t, C_p^t, x_p^t, y_p^t, u_p^t, v_p^t)$ for the system (2.1) with treatment, one needs to solve the system of equations, where the first one is (3.6) and the second is the following modification of (3.7):

$$f_C\left(\frac{T_p^t f_v\left(\frac{f_x(T_p^t)}{\mu_x}\right) g_v\left(\frac{f_y(C_p^t)}{\mu_y}\right)}{\mu_v}\right) g_C\left(\frac{f_x(T_p^t)}{\mu_x}\right) + S = \mu_C C_p^t. \tag{4.2}$$

Defining, similar to the previous section,

$$\tilde{H}_T(C) = f_C\left(\frac{f_v\left(\frac{f_x(T)}{\mu_x}\right) g_v\left(\frac{f_y(C)}{\mu_y}\right) T}{\mu_v}\right) g_C\left(\frac{f_x(T)}{\mu_x}\right) + S - \mu_C C,$$

and observing that $\tilde{H}_T'(C) = H_T'(C)$ while $\tilde{H}_T(0) = S > 0$, we conclude that for each T there is exactly one C that solves (4.2). The existence of solutions to the system (3.6)–(4.2) depends on specific properties of the functions involved in the system and parameters. We explore these solution snumerically in the next section.

5. System behavior in the biologically realistic domain. In the previous sections we explored the model in its most generic form, which delimits the scope of analysis. In order to investigate the model behavior in more detail, we make direct calculations and explore numerical solutions. To this end, we substitute the functions in system (2.1) with explicit expressions from [17] and use realistic parameters estimated in [17] and in Appendix. For the system without treatment, we check stability of the DNI steady state and find that the unique stable DI steady state exists whenever the DNI steady state is unstable. Further, we show that in any case, the stable steady state is globally attracting. For the system with treatment, i.e., $S > 0$, we find three ranges of S value, delimited by $S_{\min}$ and $S_{\max}$. For $S < S_{\min}$, the NDI steady state is unstable, and there exists one DI steady state with large T, which is globally attractive. When $S_{\min} < S < S_{\max}$, the NDI steady state becomes LAS, and an additional DI steady state with small T appears. This steady state is unstable and approximately separates the basin of attraction of the NDI steady state from that of the larger DI steady state, which retains local stability. For $S > S_{\max}$ both DI steady states disappear and the NDI steady state becomes globally attractive.

5.1. The model with explicit functions and nondimensionalization. The following functions for the system (2.1) were used in [17]:

$$r(T) = \frac{r_0}{K}(K - T), \quad f_T(x) = \frac{a_{Tx}x + e_{Tx}}{x + e_{Tx}}, \quad g_T(u) = \frac{a_T u}{u + e_T}, \quad h_T(T) = \frac{h_T}{h_T + T},$$
$$f_C(Tv) = \frac{a_{Cv}Tv}{Tv + e_{Cv}}, \quad g_C(x) = \frac{a_{Cx}x + e_{Cx}}{x + e_{Cx}}, \quad f_x(T) = g_x + a_{x,T}T, \quad f_y(C) = a_{yC}C,$$
$$f_u(y) = g_u + \frac{a_{uy}y}{y + e_{uy}}, \quad f_v(x) = \frac{a_{vx}x + e_{vx}}{x + e_{vx}}, \quad g_v(y) = \frac{a_{vy}y}{y + e_{vy}}.$$

One can reduce the number of parameters in the system by nondimensionalization. In order to achieve this, we substitute the variables and the parameters as follows:

$$\hat{T}=\frac{T}{K},\quad \hat{x}=\frac{x\mu_C}{a_{x,T}K},\quad \hat{C}=\frac{C\mu_C}{a_{C,v}},\quad \hat{y}=\frac{y\mu_C^2}{a_{y,C}a_{C,v}},\quad \hat{u}=\frac{u\mu_C}{a_{u,y}},\quad \hat{v}=\frac{v\mu_C}{a_{v,y}},$$
$$\hat{t}=t\mu_C,\quad \hat{h}_T=\frac{h_T}{K},\quad \hat{e}_{T,x}=\frac{e_{T,x}\mu_C}{K\cdot a_{x,T}},\quad \hat{a}_T=\frac{a_T a_{C,v}}{\mu_C^2},\quad \hat{e}_T=\frac{e_T\mu_C}{a_{u,y}},$$
$$\hat{e}_{C,v}=\frac{e_{C,v}\mu_C}{Ka_{v,y}},$$
$$\hat{e}_{C,x}=\frac{e_{C,x}\mu_C}{Ka_{x,T}},\quad \hat{g}_x=\frac{g_x}{Ka_{x,T}},\quad \hat{g}_u=\frac{g_u}{a_{u,y}},\quad \hat{e}_{u,y}=\frac{e_{u,y}\mu_C^2}{a_{y,C}a_{C,v}},\quad \hat{e}_{v,x}=\frac{e_{v,x}\mu_C}{Ka_{x,T}},$$
$$\hat{e}_{v,y}=\frac{e_{v,y}\mu_C^2}{a_{y,C}a_{C,v}},\quad \hat{r_0}=\frac{r_0}{\mu_C},\quad \hat{S}=\frac{S}{a_{C,v}},\quad \hat{\mu}_y=\frac{\mu_y}{\mu_C},\quad \hat{\mu}_x=\frac{\mu_x}{\mu_C},\quad \hat{\mu}_u=\frac{\mu_u}{\mu_C},$$
$$\hat{\mu}_v=\frac{\mu_v}{\mu_C}.$$

Denoting differentiation with respect to $\hat{t}$ by $'$, the system (2.1) becomes

$$\begin{aligned}
\hat{T}' &= \hat{T}\left(\hat{r}(1-\hat{T})-\hat{a}_T\hat{C}\cdot\frac{\hat{u}}{\hat{u}+\hat{e}_T}\cdot\frac{\hat{h}_T}{\hat{h}_T+\hat{T}}\cdot\frac{a_{T,x}\hat{x}+\hat{e}_{T,x}}{\hat{x}+\hat{e}_{T,x}}\right),\\
\hat{C}' &= \frac{\hat{T}\hat{v}}{\hat{T}\hat{v}+\hat{e}_{C,v}}\cdot\frac{a_{C,x}\hat{x}+\hat{e}_{C,x}}{\hat{x}+\hat{e}_{C,x}}+\hat{S}-\hat{C},\\
\hat{x}' &= \hat{g}_x+\hat{T}-\hat{\mu}_x\hat{x},\\
\hat{y}' &= \hat{C}-\hat{\mu}_y\hat{y},\\
\hat{u}' &= \hat{g}_u+\frac{\hat{y}}{\hat{y}+\hat{e}_{u,y}}-\hat{\mu}_u\hat{u},\\
\hat{v}' &= \frac{\hat{y}}{\hat{y}+\hat{e}_{v,y}}\cdot\frac{a_{v,x}\hat{x}+\hat{e}_{v,x}}{\hat{x}+\hat{e}_{v,x}}-\hat{\mu}_v\hat{v}.
\end{aligned}\tag{5.1}$$

In the following subsections we numerically explore the system (5.1) (see [17] and Appendix for parameter evaluation according to experimental and clinical literature). Note that the parameter r_0 can assume two values, one, r_{III}, is equal to the maximal growth rate of HGG grade III, and the other, r_{IV}, is equal to the maximal growth rate of HGG grade IV.

5.2. Stability of the DNI steady state and existence of DI steady states for the untreated system (5.1). Here we estimate the condition of Propositions 3 and 4. It follows from section 3 that the system (5.1) without treatment has one NDNI steady state and one DNI steady state, defined by $(\hat{T},\hat{C})=(0,0)$ and $(\hat{T},\hat{C})=(1,0)$, respectively. The NDNI steady state is always unstable, as shown in subsection 3.1. The stability of the DNI steady state is determined using Proposition 3. Propositions 3 and 4 read now as follows: $A=\frac{(\hat{a}_{C,x}(\hat{g}_x+1)+\hat{e}_{C,x}\hat{\mu}_x)(\hat{a}_{v,x}(\hat{g}_x+1)+\hat{e}_{v,x}\hat{\mu}_x)}{\hat{e}_{C,v}\hat{e}_{v,y}(\hat{g}_x+1+\hat{e}_{C,x}\hat{\mu}_x)(\hat{g}_x+1+\hat{e}_{v,x}\hat{\mu}_x)}<\hat{\mu}_y\hat{\mu}_v$ is the condition for the stability of the DNI steady state and for nonexistence of DI steady states.

The above inequality does not hold for the evaluated average parameter values. However, a reasonable change of parameters makes this condition valid. Thus, at different regions of parameter space the system can have different dynamics, due to loss of stability of the DNI steady state. More precisely, the above condition

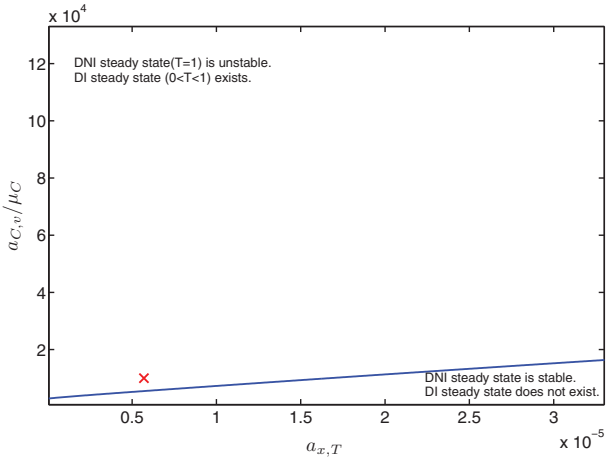

FIG. 5.1. *The separatrix (solid line) for Propositions* 3 *and* 4 *in the parameter* $(a_{x,T}, \frac{a_{C,v}}{\mu_C})$ *plane. The parameter ranges are* $a_{x,T,\min} = 2.85 \cdot 10^{-10}$, $a_{x,T,\max} = 3.42 \cdot 10^{-7}$, $\frac{a_{C,v,\min}}{\mu_{C,\max}} \approx 750$, $\frac{a_{C,v,\max}}{\mu_{C,\min}} \approx 1.33 \cdot 10^5$. *All other parameters are set to their average values. The marker* $\times$ *designates the point corresponding to the average values of* $(a_{x,T}, \frac{a_{C,v}}{\mu_C})$.

depends on 15 parameters of the unscaled system, and the equation $A = \hat{\mu}_y \hat{\mu}_v$ defines the hypersurface in the 15-dimensional box, determined by the allowable parameter ranges. This hypersurface separates the regions of stability and instability of the DNI steady state. Here we focus on three parameters that are most relevant prognostically and are expected to vary between patients, namely, $a_{x,T}$ [22], $a_{C,v}$, and μ_C [18]. Rewriting the above condition in terms of the original parameters, we get

$$\frac{a_{C,v}}{\mu_C} < \frac{\mu_v \mu_y e_{C,v} e_{v,y}}{a_{y,C} a_{v,y} K} \cdot \frac{(K a_{x,T} + g_x + e_{C,x}\mu_x)\,(K a_{x,T} + g_x + e_{v,x}\mu_x)}{(a_{C,x} K a_{x,T} + a_{C,x} g_x + e_{C,x}\mu_x)\,(a_{v,x} K a_{x,T} + a_{v,x} g_x + e_{v,x}\mu_x)}.$$

In Figure 5.1 we plot the separatrix for the last inequality in the rectangle, defined by the following ranges of the parameters: $a_{x,T,\min} \le a_{x,T} \le a_{x,T,\max}$ and $\frac{a_{C,v,\min}}{\mu_{C,\max}} \le \frac{a_{C,v}}{\mu_C} \le \frac{a_{C,v,\max}}{\mu_{C,\min}}$. The marked point on this diagram corresponds to the estimated average values of the parameters and shows that in this case the DNI steady state is unstable. Note that this condition does not depend on the value of r_0. Therefore, the separatrix is the same for both HGG grade III and grade IV.

5.3. Steady states of the untreated system (5.1). In subsection 3.3 we saw that there could exist DI steady states of the untreated system (2.1). Here we explore this issue numerically, using the explicit form of the model equations. The steady state equations results from equating the right-hand side of the system (5.1) to zero. We define for convenience $e_1 = \hat{e}_{u,y}\hat{\mu}_y$, $e_2 = \hat{e}_{v,y}\hat{\mu}_y$, $e_3 = \hat{e}_{v,x}\hat{\mu}_x$, $e_4 = \hat{e}_T \hat{\mu}_u$, $e_5 = \hat{e}_{T,x}\hat{\mu}_x$, $g_1 = \hat{g}_u e_1$, and $a_1 = a_{T,x}\hat{g}_x$, and obtain, after substitution into the first two equations:

$$\begin{aligned} &\frac{\hat{r}}{\hat{a}_T \hat{h}_T} \cdot (1 - \hat{T}) \cdot (\hat{T} + \hat{h}_T) \cdot \frac{\hat{g}_x + \hat{T} + e_5}{a_{T,x}(\hat{g}_x + \hat{T}) + e_5} = \hat{C} \cdot \frac{\hat{C} + \hat{g}_u(\hat{C} + e_1)}{\hat{C} + \hat{g}_u(\hat{C} + e_1) + e_4}, \\ &\hat{S} + \hat{T}(a_{v,x}(\hat{g}_x + \hat{T}) + e_3) \cdot (a_{C,x}(\hat{g}_x + \hat{T}) + e_7) \\ &\qquad = \hat{T}\hat{C}(a_{v,x}(\hat{g}_x + \hat{T}) + e_3) + e_6(\hat{C} + e_2)(\hat{g}_x + \hat{T} + e_3)(\hat{g}_x + \hat{T} + e_7) \end{aligned} \tag{5.2}$$

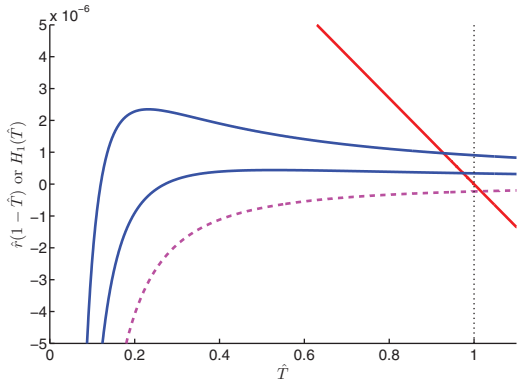

FIG. 5.2. *The graphic solution to the equation for $\hat{T}$ resulting from* (5.2). *The descending straight line is the plot of $\hat{r}_0(1-\hat{T})$, for which we took $\hat{r}_0 = \hat{r}_{III}/10^4$ to enhance the visualization. The other three curves are plots of $H_1(\hat{T})$ for values of $a_{C,v} = 0.1, 100, 200$. The solutions are sought in the range $0 \le \hat{T} \le 1$ (to the left of the vertical dotted line). It can be seen that for $a_{C,v} = 0.1$ (below the separatrix) no positive solutions exist (dotted curve) while crossing the separatrix results in bifurcation from $\hat{T} = 1$ (solid curves).*

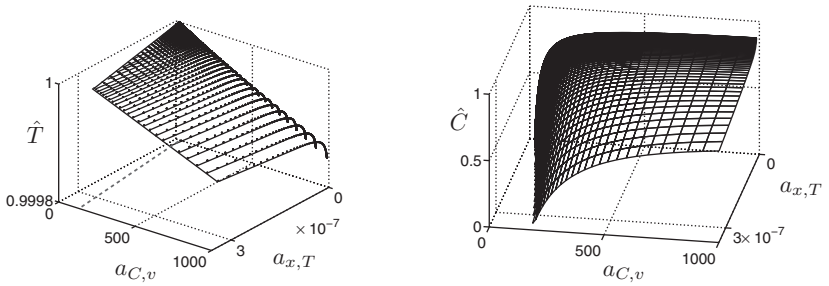

FIG. 5.3. *DI steady states of the HGG grade III, defined by $r_0 = r_{III} = 0.00035h^{-1}$, as a function of the values of $a_{C,v}$ and $a_{x,T}$, for $\hat{T}$ (left) and for $\hat{C}$ (right). The separatrix appears as a straight line in the $(a_{C,v},a_{x,T})$-plane. The DI steady state appears above the separatrix in the $(a_{C,v},a_{x,T})$-plane (see Figure* 5.1).

Letting $\hat{S} = 0$, the second equation is linear in $\hat{C}$ and can be substituted into the first equation yielding a polynomial equation of the sixth degree for $\hat{T}$. This equation can be put into the form $\hat{r}_0(1-\hat{T}) = H_1(\hat{T})$, H_1 being a rational function. As shown in subsection 3.3, DI steady states are expected to be found only in the regions of the parameter space where the condition of Proposition 3 does not hold. Indeed, numerical studies show that in the box defined by the estimated parameter ranges in the $(a_{T,x}, a_{C,v})$-plane, there are no positive solutions for (5.2) below the separatrix (see Figure 5.1), while above the separatrix there is exactly one positive solution. Crossing the separatrix from below in this box creates a new steady state, which bifurcates from the DNI steady state, $\hat{T} = 1, \hat{C} = 0$. As an example, we show the graphic solution to this equation for several values of $a_{C,v}$ (Figure 5.2). An increase in $a_{C,v}$ leads to the appearance of a positive solution.

The steady states of the untreated system, for HGG grade III, are shown on a logarithmic-scale grid of $a_{C,v}$ and $a_{x,T}$ (Figure 5.3). The grid points were all the points in the set $\{e^{0.075\cdot i} | \frac{\ln 7}{0.075} \le i \le \frac{\ln 700}{0.075}, i \in \mathbb{Z}\} \times \{e^{0.1\cdot i} | \frac{\ln 5.61\cdot 10^{-8}}{0.075} \le i \le \frac{\ln 5.61\cdot 10^{-8}}{0.075}, i \in \mathbb{Z}\}$. For the HGG grade IV, defined by $r_0 = r_{IV}$, the plot is similar.

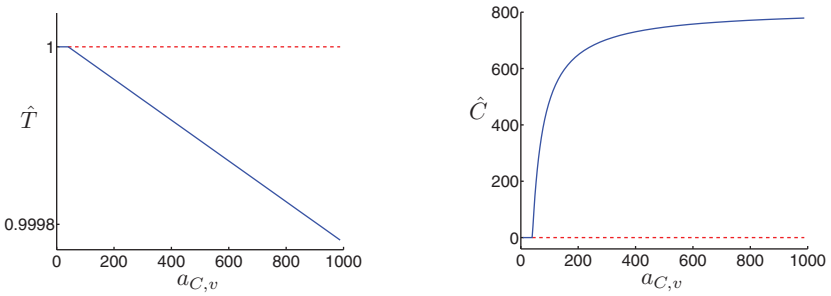

FIG. 5.4. *The bifurcation diagram for the steady states of the HGG grade* III, *defined by* $r_0 = r_{III} = 0.00035h^{-1}$, *depending on the value of* $a_{C,v}$ *for* $\hat{T}$ *(left) and* $\hat{C}$ *(right); all other parameters are constant. After crossing the separatrix, a stable DI steady state appears, while the DNI steady state becomes unstable.*

We see that a single DI steady state exists in the parameter region, allowed by Proposition 3. It bifurcates from the DNI steady state, $\hat{T} = 1$, $\hat{C} = 0$ upon crossing the separatrix in the $(a_{x,T}, a_{C,v})$-plane, simultaneously with the loss of stability of the DNI state. This loss of stability at the bifurcation point suggests that the DI steady state is LAS whenever it exists. To check this, we have computed the value of the DI steady state and the eigenvalues of the Jacobi matrix for the points on the grid defined above. Computation shows that at all the points in the grid where the DI steady state exists (i.e. above the separatrix) it is LAS. In Figure 5.4 we present the steady state diagrams for HGG grade III, as dependent on $a_{C,v}$ only, with all other parameters being constant. The diagram looks similar for HGG grade IV, with the bifurcation occurring for the same value of $a_{C,v}$.

5.4. Global behavior of the untreated system (5.1). Upon establishing the steady states and their local stability properties, we study the global behavior of the system by computer simulations. We have simulated the system (5.1) for $\hat{S} = 0$, at each point of the grid in the $(a_{T,x}, a_{C,v})$-plane for which the steady states and their stability were determined in the previous subsection. For each grid point, 50 simulations of the scaled system (5.1) were performed for both HGG grade III and grade IV. The initial data for each simulation are as follows: the values of $\hat{T}(0)$ and $\hat{C}(0)$ are chosen randomly in the intervals $[0, 1]$ and $[0, 2]$, respectively, while the other four variables are given values, computed from steady state equations using $\hat{T}(0)$ and $\hat{C}(0)$. This choice is based on the observation that, when choosing the initial data for $\hat{x}$, $\hat{y}$, $\hat{u}$, and $\hat{v}$ in the appropriate ranges (given by Proposition 1), these variables converge very fast to, approximately, their steady state values for the current values of $\hat{T}(t)$ and $\hat{C}(t)$. In all the simulations, the system converged to the appropriate LAS steady state, as defined by the parameter choice.

5.5. Stability of the NDI steady state for the treated system (5.1). Now we turn to the analysis of the treated system. Here we determine the range of CTLs infusion rate S, which satisfies the condition of Proposition 5. This proposition reads now:

$$\hat{S} \cdot \frac{\hat{a}_T \left(\hat{S}(\hat{g}_u + 1) + \hat{g}_u \hat{\mu}_u \hat{e}_{u,y} \right)}{\hat{S}(\hat{g}_u + \hat{e}_T \hat{\mu}_u + 1) + (\hat{g}_u + \hat{e}_T \hat{\mu}_u)\hat{\mu}_u \hat{e}_{u,y}} > \frac{(\hat{g}_x + \hat{e}_{T,x} \hat{\mu}_x)\hat{r}}{\hat{a}_{T,x} \hat{g}_x + \hat{e}_{T,x} \hat{\mu}_x} \tag{5.3}$$

is the condition for local stability of the NDI steady state $(0, C_{st}, x_{st}, y_{st}, u_{st}, v_{st})$.

The threshold value $\hat{S}_{loc}$ of $\hat{S}$ for this inequality is given by a quadratic equation, which has one positive root, so that for $\hat{S} > \hat{S}_{loc}$, the condition of Proposition 5 holds. For the evaluated parameter values one can estimate these thresholds for HGG grade III (using $r_0 = 0.00035h^{-1}$):
$\hat{S}_{loc,III} \approx 0.41$ for the nondimensional system and
$S_{loc,III} \approx 0.41 \cdot a_{C,v} \approx 30.4 cells/h$ for the estimated parameter values;
and for HGG grade IV (using $r_0 = 0.001h^{-1}$):
$\hat{S}_{loc,IV} \approx 1.14$ for the nondimensional system and
$S_{loc,IV} \approx 1.14 \cdot a_{C,v} \approx 84.7 cells/h$ for the estimated parameter values.

Similar to the previous subsection, we wish to evaluate these results as a function of the parameters $a_{x,T}$, $a_{C,v}$, and μ_C. Representing the expression for $\hat{S}$ in the original parameters, one can see that the first two parameters do not influence its value, while for the latter the dependence is linear. Thus, an increase in the CTL life-span linearly reduces the value of the minimal infusion rate required for stability of the NDI steady state.

Further, we can estimate the sufficient condition for the global stability, as given in Remark 1. This inequality differs only in estimation of its right-hand side. Thus, we obtain

$$\hat{S} \cdot \frac{\hat{a}_T \left(\hat{S}(\hat{g}_u + 1) + \hat{g}_u \hat{\mu}_u \hat{e}_{u,y} \right)}{\hat{S}(\hat{g}_u + \hat{e}_T \hat{\mu}_u + 1) + (\hat{g}_u + \hat{e}_T \hat{\mu}_u)\hat{\mu}_u \hat{e}_{u,y}} > \frac{\hat{r}(\hat{g}_x + 1 + \hat{e}_{T,x}\hat{\mu}_x)(\hat{h}_T + 1)}{(\hat{a}_{T,x}(\hat{g}_x + 1) + \hat{e}_{T,x}\hat{\mu}_x)\,\hat{h}_T}.$$

For the esimated parameter values (see Table 1) we compute for HGG grade III:
$\hat{S}_{glob,III} \approx 7.34 \cdot 10^4$ and $S_{glob,III} \approx 5.44 \cdot 10^6 cells/h$;
for HGG grade IV:
$\hat{S}_{glob,IV} \approx 2.05 \cdot 10^5$ and $S_{glob,IV} \approx 1.52 \cdot 10^7 cells/h$.
These values are close to the current clinical limits (see Discussion). In the next subsection these estimations are improved to obtain clinically achievable protocols.

5.6. Steady states of the treated system (5.1). Now we consider the DI steady states of the treated system. These are given by the same equations as in subsection 5.3, with $\hat{S} > 0$. In this case we fixed all the parameters at their average values, but allowed $\hat{S}$ to vary from 0 to 10^5. For positive $\hat{S}$ the second equation in (5.2) yields a quadratic equation in $\hat{C}$, which has exactly one positive root. Substitution of the latter into the first equation leads to a high-degree equation in $\hat{T}$, including polynomial terms and square root, whose solution we explored numerically. Similar to the untreated case, the first equation takes the form $\hat{r}_0(1 - \hat{T}) = H_2(\hat{T})$, with H_2 depending also on $\hat{S}$.

To clarify the behavior of the steady state as depending on $\hat{S}$, we show the graphic solution to the latter equation for HGG grade III in Figure 5.5. The value of $\hat{S}$ determines the number of solutions of this equation. For small S there exists one positive solution, and an additional positive solution appears for larger values of $\hat{S}$ (Figure 5.5, left). When $\hat{S}$ becomes higher than some threshold $\hat{S}_{\max}$, both positive solutions disappear (Figure 5.5, right). A similar pattern is observed for HGG grade IV. Note that the values of the thresholds are different for different tumor grades. For HGG grade III, the first threshold for $\hat{S}$ (appearance of second DI steady state) is $\hat{S}_{min,III} \approx \hat{S}_{loc,III} \approx 0.4$, while the second threshold (disappearance of both steady states) is $\hat{S}_{max,III} \approx 1.903 \cdot 10^4$. For grade IV, these values are $\hat{S}_{min,IV} \approx \hat{S}_{loc,IV} \approx 1.14$ and $\hat{S}_{max,IV} \approx 5.166 \cdot 10^4$, respectively.

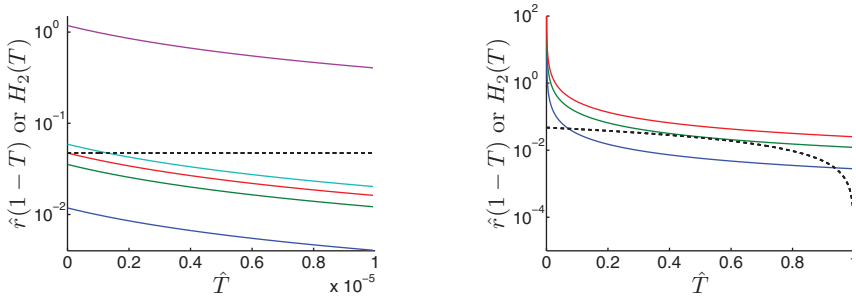

FIG. 5.5. *The graphic solution to the first steady state equation of the treated system* (5.2)*, for HGG grade III, defined by* $r_0 = r_{III} = 0.00035h^{-1}$*. The y-axis is at logarithmic scale. The dashed line is the plot of* $\hat{r}_0(1-\hat{T})$*. The other curves are plots of* $H_2(\hat{T})$ *for different values of* $\hat{S}$ *(all other parameters are at their average values). The left figure shows the appearance of small DI steady state (for* $\hat{S} \approx 0.4$*). The right figure shows the bifurcation, by which both DI steady states disappear (for* $\hat{S} \approx 2 \cdot 10^5$*).*

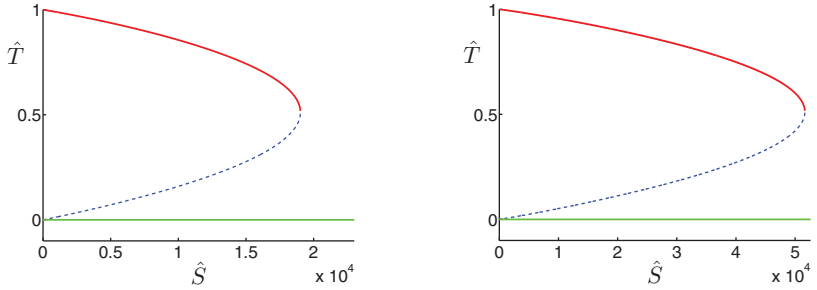

FIG. 5.6. *Steady state diagram for* $\hat{T}$ *for grade* III *(left) and grade* IV *(right). For small* $\hat{S}$ $(\hat{S} < \hat{S}_{\min})$ *the NDI steady state* $\hat{T} = 0$*,* $\hat{C} = \hat{S}$*, is unstable, while the only DI steady state is LAS. For intermediate values of* $\hat{S}$ $(\hat{S}_{\min} < \hat{S} < \hat{S}_{\max})$*, the NDI steady state is LAS, as well as the larger DI steady state, while the smaller DI steady state is unstable. For larger* $\hat{S}$ *both DI steady states disappear, while the NDI steady state remains LAS.*

In Figure 5.6 we show the steady state diagram for $\hat{T}$ as a function of $\hat{S}$, for both HGG grade III and grade IV. The diagram shows, as expected, that for small values of $\hat{S}$, there is only one DI steady state, with $\hat{T}$ somewhat smaller than 1. When S becomes larger than $\hat{S}_{\min}$, an additional DI steady state appears, bifurcating from the NDI steady state. When $\hat{S}$ increases, the two DI steady states get closer in values of $\hat{T}$, and for $\hat{S}$ above $\hat{S}_{\max}$ they both disappear. Note that the first threshold in $\hat{S}$ in this diagram indeed coincides with $\hat{S}_{loc}$ for both HGG grade III and grade IV. Proposition 5 and section 5.5 suggest that for $S < S_{loc}$ the only DI steady state should be LAS, while for larger S the DI steady state with larger T should retain stability and the DI steady state that bifurcates from the NDI steady state should be unstable (while the NDI steady state becomes LAS, as was proven). To check this, we have computed the eigenvalues of the Jacobi matrix for the DI steady states, for both HGG grade III and grade IV, and for values of $\hat{S}$ ranging from 0 to the maximal value for which DI steady states exist. Figure 5.6 includes also the stability results, which confirm the local stability of the maximal DI steady state, whenever it exists and the instability of the second, minimal one, whenever it exists.

5.7. Global behavior of the treated system (5.1). We turn to explore the global behavior of the treated system. We define three intervals of $\hat{S}$, according to

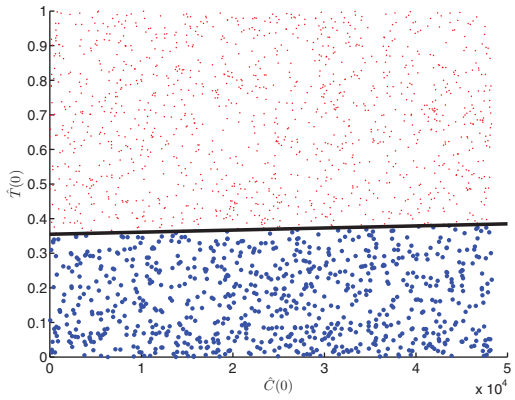

FIG. 5.7. *Basins of attraction for the treated system with two LAS steady states. The large points are initial values of* $(\hat{T}, \hat{C})$ *from which the system converges to the NDI steady state. The small points are initial values from which the system converges to the DI steady state. In these simulations,* $\hat{S} \approx 4.8 \cdot 10^4$, $\hat{r}_0 = \hat{r}_{IV}$.

the number and characterization of the steady states. First, it was proven that for $\hat{S} > \hat{S}_{glob}$, the unique steady state is globally stable (see Remark 1). Therefore, we consider only $\hat{S}$ below this value. The first interval is defined by $0 \le \hat{S} < \hat{S}_{\min}$. In this case, there exist an unstable NDI steady state and a positive, locally stable DI steady state. We have performed 200 simulations with randomly chosen initial conditions (as above for the simulations of the untreated system), for every value of $\hat{S}$ in the set $\{0.1, 0.39, 0.4\}$ for HGG grade III, and for every value of $\hat{S}$ from the set $\{0.1, 0.4, 0.7, 1, 1.13, 1.14\}$ for HGG grade IV. Convergence to the DI steady state was observed in all the simulations, suggesting its global stability.

The second interval is defined by $\hat{S}_{\min} \le \hat{S} \le \hat{S}_{\max}$. In this interval, for each $\hat{S}$, there exist two DI steady states. The computation in the previous subsection shows that the NDI and the larger DI steady states are LAS. Therefore, we expect that there exist two sets: U_1 of the initial values for which the system converges to the NDI steady state, and U_2 of the initial values for which the system converges to the stable DI steady state. Similar to the first interval, we have performed 200 simulations for each $\hat{S}$ value in the set $\{0.41, 0.42, 0.43, 4200, 7200, 9200, 1.8 \cdot 10^4, 1.901 \cdot 10^4, 1.902 \cdot 10^4\}$ for HGG grade III, and for each $\hat{S}$ value in the set $\{1.15, 1.16, 1.17, 1.19, 2, 230, 730, 38300, 48300, 50300, 51600, 51640, 51650\}$ for HGG grade IV. These values are chosen to represent intermediate and border values of the interval $(S_{\min}, S_{\max})$. Simulations show that any initial point belongs to one of the sets U_1 and U_2 (i.e., there are no types of behavior other than convergence to a stable steady state). To visualize the separation, we consider the projection of these sets on the (T, C)-plane. We have performed 2000 simulations for one value of $\hat{S} \approx 4.8 \cdot 10^4$ for HGG grade IV. In Figure 5.7 we plot the initial points on the $(\hat{T}, \hat{C})$-plane in two sizes: the initial points, starting from which the system converges to the NDI steady state are large, while the initial points, from which the system converges to the stable DI steady state are small. It is clearly seen that the asymptotic behavior primarily depends on the value of $\hat{T}(0)$, the threshold value being approximately equal to the unstable DI steady state value of $\hat{T}$, corresponding to $\hat{S}$.

The third interval is defined by $\hat{S}_{\max} \le \hat{S} \le \hat{S}_{glob}$. In this interval only the NDI steady state exists, which is LAS, and we wish to verify its global stability. Using

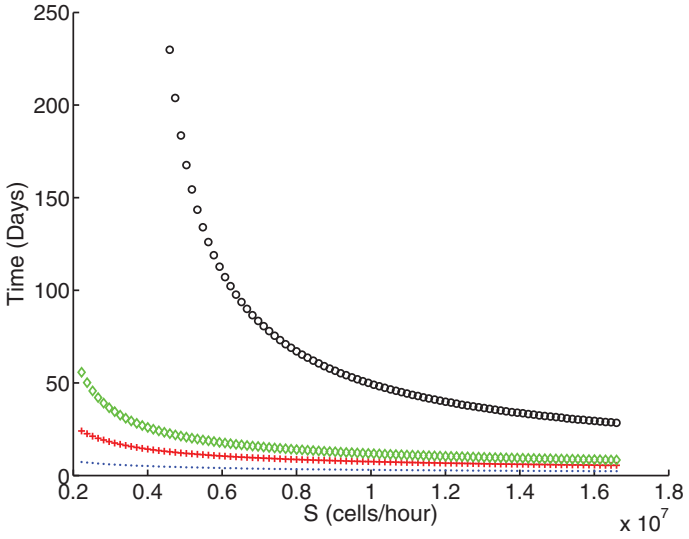

FIG. 5.8. *The result of time to cure (TTC, a first time point at which T dropped below 10^{-11}) estimation for grade IV tumor. We simulated treatment of the tumor from four different initial sizes $T(0) = 0.01$ (dots), 0.05 (pluses), 0.1 (rhombuses), 0.5 (open circles), setting $C(0) = 0$. For each initial tumor size, TTC was estimated as a function of S, producing a curve of dependence of TTC (y-axis) on S (x-axis).*

Lemma 1 in [16], we see that if for some $\hat{S} = \hat{S}_e$, the tumor is eliminated, then, for each $\hat{S} > \hat{S}_e + 1$, it is also true for the same initial values, since in the scaled system $f_C(\hat{T}\hat{v})g_C(\hat{x}) \leq 1$. Thus, for grade III we have verified that for $\hat{S} = 1.903 \cdot 10^4$, the tumor is eliminated for any initial data in the relevant range, as well as for $\hat{S} = 1.9031 \cdot 10^4$. Similarly, for grade IV we have verified tumor elimination for $\hat{S} = 5.166 \cdot 10^4$ and for $\hat{S} = 5.1661 \cdot 10^4$. This suggests global stability of the NDI steady state for $\hat{S} > \hat{S}_{\max}$ which improves the estimation given by Remark 1.

5.8. Estimation of the time to cure. In view of the above results, one can see that for any initial tumor size, there exists a value of S, starting from which the constant infusion treatment succeeds in eliminating the tumor. However, in practice, it is important to determine the duration of treatment required for tumor elimination, as excessive treatment can lead to unnecessary side effects. Therefore, we explore the time to cure (TTC) predicted by our model. To this end, we have simulated treatment of HGG grade III and grade IV tumors with different initial sizes, namely, $\hat{T}(0) = 0.01, 0.05, 0.1$, and 0.5. These values are chosen to represent the span of possible detection sizes for HGG (from $\sim$ 1cm, corresponding to $\sim 10^9 cells$ to late detection corresponding to half of the maximal size). In all cases we assume $\hat{C}(0) = 0$. The initial values for all other variables are set at quasi-equilibrium values. The TTC is defined as the first time point at which $\hat{T}(t) < 1 \cdot 10^{-11}$ (i.e., there is less than one tumor cell present).

In Figure 5.8 we show the dependence of TTC on the value of $\hat{S}$, for different initial tumor sizes, for grade IV. We see that for each initial tumor size, the TTC monotonically decreases when increasing the infusion rate. It is apparent that larger initial tumor size requires longer treatment. Intermediate infusion rate will never be sufficient for eliminating larger tumors; however, by significantly increasing the infusion rate even such a tumor can be eliminated in a reasonable time.

Discussion. In this work we analyzed a mathematical model for HGG–immune system interactions, in the untreated setting and under CTL infusion at a constant rate S. In the untreated setting we found that the system always has one globally attracting steady state. Depending on parameter values, this can be either DNI steady state, with $T = K$, or DI steady state, with $T < K$, the value of T being very close to K for the realistic parameter values. For the treated setting, we identified three intervals of S values, separated by two thresholds, $S_{\min}$ and $S_{\max}$. For $S < S_{\min}$ the system always converges to the unique DI steady state, with large tumor size T. For $S_{\min} < S < S_{\max}$ two attracting steady states exist. One is NDI steady state, and the other is DI steady state, having large T. In addition, there exists one unstable DI steady state, with smaller T. The NDI steady state attracts solutions with a small enough initial value of T. The stable DI steady state attracts other solutions. Upon an increase in S, the basin of attraction of the NDI steady state increases. For $S > S_{\max}$, only the NDI steady state exists and it is globally attracting, ensuring that the tumor will eventually be eradicated.

Our model predicts tumor growth to a large size, either at the system's carrying capacity or close to it, if no treatment is administered. The clinical meaning of this is that an untreated brain tumor will inevitably grow to a maximal limit size, since the natural immune response against it is too weak. Proposition 3 shows that an increase in the immune response by manipulation of the pro-immune or the immune suppressive parameters can lead to a decrease in the steady state tumor load, this decrease being insignificant (less than 0.01%) within the scope of realistic parameter values, as shown in subsection 5.3. Nevertheless, a therapy which can cause a major change in these parameters, e.g., by an increase in CTL life-span [13], can lead to tumor control. Such a mode of treatment has led to trials with immortalized CTLs [11, 26, 29] which unfortunately ended in genetic instability [25]. Note also that the NDI steady state is unstable without treatment, implying that the natural immune response cannot guarantee tumor eradication. Therefore, after surgical or drug-induced tumor reduction to an undetectable size, one should consider maintaining a constant level of CTL infusion to ensure the tumor demise. Practically, this may require developing techniques to maintain the viability of T cells. This can also be possibly achieved by vaccination (e.g., using whole cell tumor vaccines [27], or dendritic cell vaccine [8]), which will guarantee the presence of sentinels in the brain.

Analysis of the treated case shows that treatment outcomes depend on infusion intensity, with three distinct intervals for the infusion rate S. These intervals are defined by two thresholds, $S_{\min}$ and $S_{\max}$. When infusion rate is less than $S_{\min}$, immunotherapy is never sufficient. Therefore, any treatment of low T cell infusion will be futile. Medium infusion rate, somewhat larger than $S_{\min}$, ensures the existence of the NDI steady state, $T = 0, C = \frac{S}{\mu_C}$, which is LAS. This means that when the initial tumor size is within a stable neighborhood of the NDI steady state, tumor decline toward zero is guaranteed. Clinically, this requires a reduction of tumor size prior to immunotherapy. Such a reduction can occur postsurgery, or concomitantly with chemotherapy, which could provide a suitable window of opportunities for medium-intensity immunotherapy. On the other hand, there exists a critical initial tumor size, beyond which the immunotherapy treatment will only ensure a partial reduction of tumor load. An increase in infusion rate entails an increase in this critical initial tumor size as well as a reduction of the larger steady state, implying possibility of tumor control even when the cure is unattainable. Such behavior can be compared to tumor stable partial response to the treatment. When the infusion rate is higher than $S_{\max}$, a curative globally attractive steady state exists. Thus, $S_{\max}$ is the min-

imal infusion rate that ensures cure from any initial tumor load, if maintained long enough. Note that this threshold value, as computed in subsection 5.6, turns out to be at least by one order of magnitude smaller than the value S_{glob} estimated in Remark 1, for both HGG grade III and grade IV. The value of $S_{\max}$ and the range of time to cure, estimated in subsection 5.8 are clinically feasible [31].

We conclude our analysis by estimating the duration of treatment necessary for such adoptive cellular therapy to cure patients of different initial tumor sizes. Our results suggest that the estimated time frames (see Figure 5.8) are well within clinical feasibility.

Clinical trials in cellular immunotherapy have shown some side effects, ranging from influenza-like symptoms [20] to autoimmune symptoms such as Vitligo and Uveitis [9]. The severity of the symptoms seems to be dose-dependent. Therefore, we anticipate that high and prolonged dosages may be limited by the severity and duration of such symptoms. However, such symptoms are usually not considered lethal. Mathematical methods for optimizing treatment strategies, considering both efficacy and toxicity have been developed [1], and can be considered here, upon sufficient information.

Dynamical models by ODEs of tumor–immune system interactions have been explored in the past by different authors (see Introduction). Our model is new in explicitly considering the role of MHC receptors as immune reaction mediators, and in focusing on a specific type of brain tumor and on a novel mode of cellular treatment. These specificities are reflected in the estimated parameters, showing innate CTL recruitment to be practically ineffective. This may be the reason why no oscillations, limit cycles, or tumor dormancy are observed in our model, within the biologically relevant parameter ranges, as compared to [14] or [21]. The ability to evaluate model parameters endows it with the power to tailor immunotherapy to an individual patient. In line with the previous results [6, 7, 14], we found that the treatment intensity and the initial tumor burden are crucial factors in determining the treatment success.

There is no doubt that the translation of in vitro parameter evaluations, such as the survival time of T cells or their lytic activity, into the clinical setting of adoptive T cell therapy requires caution. However, in practice, the design of novel treatment strategies is at the discretion of the clinical investigators, based on their experience and intuition. Mathematical analysis can guide experimentalists by taking into account quantitative and qualitative information, and integrating it beyond the immediate and run-of-the-mill implications. In this work, we have derived through theoretical analysis, a clinically practical treatment parameter, namely, T cell infusion rate. This rate can be calculated on a per-patient basis, using clinical measurements, such as tumor size. Our model can assist the clinician in overcoming two major obstacles in successfully applying chemotherapy. One is in patient screening: usually there is no attempt in clinical trials to sort patients by accurately quantifying tumor load. We deem this estimation necessary to determine the minimal required T cell dose. Our work implies that some patients may receive a suboptimal T cell dose. These patients will require higher T cell infusion rate. The second obstacle is that currently there is no correlation between a patient's response to T cell therapy and the regimen he/she is prescribed in the clinical trial; according to our analysis, partial responders should be prescribed a more intensive T cell regimen.

In this work we lay the foundations for a rational patient-tailored design of adoptive T cell immunotherapy by explicitly finding infusion rates, for which stable curative steady state can exist. Moreover, we determine the values of infusion rate S for which tumor eradication will be theoretically possible from any initial tumor size. Such ra-

tional planning of adoptive T cell therapy will hopefully aid immunotherapy research. To verify our model, it is mandatory to conduct in vitro experiments, animal trials, and ultimately clinical trials and compare their results to the model predictions.

Appendix. Parameter estimation. For most of the model parameters, we used the values estimated in [17]. Here we give the estimation for the few of the parameters that were given different values, as well as range estimation for the relevant parameters. The parameters related to the production and effect of TGF-β and IFN-γ were translated from weight into concentration units, in line with the explanation in section 2. Parameter a_T was estimated differently from [17], following the assumption that no effect of large tumor mass existed in vitro. Parameter h_T was estimated in such a way that allowed reproduction of the results of clinical studies, as in [17]. All the parameters' values are summarized in Table 1.

Cytokine production rates, $a_{y,C}$ and g_x. In [17] we estimated the production rate of the IFN-γ quantity by a single CTL, $a_{\gamma,C} \approx 1.02 \cdot 10^{-4} pg/(cell \cdot h)$. The calculation was based on the estimated constant CSF volume, 150 ml. Therefore, translating IFN-γ into concentration units gives $a_{y,C} \approx \frac{1.02 \cdot 10^{-4}}{150} \approx 6.8 \cdot 10^{-7} pg/(ml \cdot cell \cdot h)$. Similar consideration for base level production of TGF-β yields $g_x \approx \frac{6.33 \cdot 10^4}{150} \approx 422 pg/(ml \cdot h)$.

TABLE 1
The estimation and the scaling of the data.

Parameter	Estimated value	Units	Rescaled value
r_{III}	$3.5 \cdot 10^{-4}$	h^{-1}	$4.72 \cdot 10^{-2}$
r_{IV}	10^{-3}	h^{-1}	$1.35 \cdot 10^{-1}$
K	10^{11}	$cells$	1
a_T	$1.54 \cdot 10^{-7}$	$cells^{-1} \cdot h^{-1}$	$2.08 \cdot 10^{-1}$
e_T	50	$rec/cell$	$1.28 \cdot 10^{-1}$
$a_{T,x}$	$6.9 \cdot 10^{-1}$	—	$6.9 \cdot 10^{-1}$
$e_{T,x}$	66.7	pg	$1.3 \cdot 10^{-4}$
h_T	$5.2 \cdot 10^5$	$cells$	$5.2 \cdot 10^{-6}$
μ_C	$7.41 \cdot 10^{-3}$	h^{-1}	1
$a_{C,v}$	74.1	$cells/h$	1
$e_{C,v}$	10^{14}	rec	$8.54 \cdot 10^{-4}$
$a_{C,x}$	$7.94 \cdot 10^{-1}$	—	$7.94 \cdot 10^{-1}$
$e_{C,x}$	66.7	pg	$1.3 \cdot 10^{-4}$
μ_x	6.93	h^{-1}	$9.35 \cdot 10^2$
g_x	422	$pg/(cell \cdot h)$	$1.11 \cdot 10^{-1}$
$a_{x,T}$	$3.79 \cdot 10^{-8}$	$pg/(cell \cdot h)$	1
μ_y	$1.02 \cdot 10^{-1}$	h^{-1}	13.8
$a_{y,C}$	$6.8 \cdot 10^{-7}$	$pg/(cell \cdot h)$	1
μ_u	$1.44 \cdot 10^{-2}$	h^{-1}	1.94
g_u	1.44	$rec/(cell \cdot h)$	0.5
$a_{u,y}$	2.89	$rec/(cell \cdot h)$	1
$e_{u,y}$	$2.25 \cdot 10^3$	pg	$2.46 \cdot 10^3$
μ_v	$1.44 \cdot 10^{-2}$	h^{-1}	1.94
$a_{v,y}$	$8.67 \cdot 10^3$	$rec/(cell \cdot h)$	1
$e_{v,y}$	9.47	pg	10.3
$a_{v,x}$	$1.2 \cdot 10^{-2}$	—	$1.2 \cdot 10^{-2}$
$e_{v,x}$	667	pg	$1.3 \cdot 10^{-3}$

Range for production rate of TGF-β by a single tumor cell, $a_{x,T}$. As explained in [17], the level of TGF-β in a patient is expected to be 10 times higher than in a healthy subject. We take its range to be between 65 and 5000 pg/ml, while the average value is $609pg/ml$. Using the equation for TGF-β at steady state, we obtain the following range:
$a_{x,T,\min} = \frac{65 \cdot \mu_x - g_x}{K} \approx 2.85 \cdot 10^{-10} pg/(ml \cdot cells \cdot h)$.
$a_{x,T,\text{norm}} = \frac{609 \cdot \mu_x - g_x}{K} \approx 3.79 \cdot 10^{-8} pg/(ml \cdot cells \cdot h)$.
$a_{x,T,\max} = \frac{5 \cdot 10^3 \cdot \mu_x - g_x}{K} \approx 3.42 \cdot 10^{-7} pg/(ml \cdot cells \cdot h)$.

Parameters of TGF-β effect. In [17], the effect of TGF-β on CTL killing efficacy was expressed as $\frac{a_{T,\beta} F_\beta + e_{T,\beta}}{F_\beta + e_{T,\beta}}$. In the present work we define $x = \frac{F_\beta}{V}$, where $V = 150ml$, the CSF volume, and the expression becomes $\frac{a_{T,\beta} x + \frac{e_{T,\beta}}{V}}{x + \frac{e_{T,\beta}}{V}}$. Therefore, we have $a_{T,x} = a_{T,\beta} \approx 0.69$ and $e_{T,x} = \frac{e_{T,\beta}}{V} \approx 66.7 pg/ml$. In a similar manner, $e_{C,x} = \frac{e_{C,\beta}}{V} \approx 66.7 pg/ml$ and $e_{v,x} = \frac{e_{v,\beta}}{V} \approx 667 pg/ml$.

Parameters of IFN-γ effect. Similarly, the effect of IFN-γ on MHCI production was expressed in [17] as $\frac{a_{u,\gamma} F_\gamma}{F_\gamma + e_{u,\gamma}}$. Defining, as above, $y = \frac{F_\gamma}{V}$, we have $a_{u,y} = a_{u,\gamma} \approx 2.89 rec/(cell \cdot h)$ and $e_{u,y} = \frac{e_{u,\gamma}}{V} \approx 2.25 \cdot 10^3 pg/ml$. In a similar manner, $e_{v,y} = \frac{e_{v,\gamma}}{V} \approx 9.47 pg/ml$.

Maximal efficacy of a CTL, a_T. Wick et al. [30] report that a CTL kills 0.7–3 target cells per day. A mean value of 1.85 target cells per CTL per day gives the rate of $0.0771h^{-1}$. The experiment was done with $5 \cdot 10^5$ target $cells/ml$ in 2 ml wells. For this calculation we assumed maximal killing efficacy of CTLs, i.e., no effects of TGF-β or large tumor mass. Substituting the former values into $a_T \cdot T = 0.0771h^{-1}$, we got $a_T = 1.54 \cdot 10^{-7} cell^{-1} h^{-1}$.

Parameter for CTL efficacy saturation due to large tumor size, h_T. We estimated this value to be $5.2 \cdot 10^5$ $cells$.

Death rate of CTLs, μ_C. Taylor et al. [28] find CTL half-life to be 3 to 3.9 days. In [17] we used the value of $7.41 \cdot 10^{-3}$ which corresponds to the half-life of 3.9 days. For range estimation we used the values of 3 and 4 days and thus obtained:
$\mu_{C,\min} = \frac{ln2}{96h} \approx 7.22 \cdot 10^{-3} h^{-1}$, $\mu_{C,\max} = \frac{ln2}{72h} \approx 9.62 \cdot 10^{-3} h^{-1}$.

Maximal effect of M_{II} on CTL recruitment, $a_{C,v}$. The numbers of endogenous CTLs in the untreated case are estimated to be 10^3–10^5 $cells$ [9]. Therefore, we estimate the maximal recruitment rate as follows:
$a_{C,v,\min} = 10^3 \cdot \mu_{C,\min} \approx 1000 \cdot 7.22 \cdot 10^{-3} = 7.22 cells/h$,
$a_{C,v,\text{norm}} = 10^4 \cdot \mu_{C,\text{norm}} \approx 10^4 \cdot 7.41 \cdot 10^{-3} = 74.1 cells/h$,
$a_{C,v,\max} = 10^5 \cdot \mu_{C,\max} \approx 10^5 \cdot 9.62 \cdot 10^{-3} = 962 cells/h$.

Acknowledgments. The authors would like to thank Prof. Carol Kruse and Dr. Matthias Wöelfl, for helpful discussions and insights. U.F.

REFERENCES

[1] Z. Agur, R. Hassin, and S. Levy, *Optimizing chemotherapy scheduling using local search heuristics*, Oper. Res., 54 (2006), pp. 829–846.
[2] J.C. Arciero, T.L. Jackson, and D.E. Kirschner, *A mathematical model of tumor-immune evasion and siRNA treatment*, Discrete Contin. Dyn. Syst. Ser. B, 4 (2004), pp. 39–58.
[3] A. Cappuccio, M. Elishmereni, and Z. Agur, *Cancer immunotherapy by interleukin-21. Potential treatment strategies evaluated in a mathematical model*, Cancer Res., 66 (2006), pp. 7293–7300.
[4] A. Cappuccio, M. Elishmereni, and Z. Agur, *Optimization of Interleukin-21 immunotherapeutic strategies*, J. Theoret. Biol., 248 (2007), pp. 259–266.

[5] C. Coppin, *Immunotherapy for renal cell cancer in the era of targeted therapy*, Expert Rev. Anticancer Ther., 8 (2006), pp. 907–919.
[6] L.G. de Pillis, A.E. Radunskaya, and C.L. Wiseman, *A validated mathematical model of cell-mediated immune response to tumor growth*, Cancer Res., 65 (2005), pp. 7950–7958.
[7] L.G. de Pillis, W. Gu, and A.E. Radunskaya, *Mixed immunotherapy and chemotherapy of tumors: Modeling, applications and biological interpretations*, J. Theoret. Biol., 238 (2006), pp. 841–862.
[8] S. de Vleeschouwer, M. Rapp, R.V. Sorg, H.J. Steiger, W. Stummer, S. van Gool, and M. Sabel, *Dendritic cell vaccination in patients with malignant gliomas: Current status and future directions*, Neurosurg., 59 (2006), pp. 988–1000.
[9] M.E. Dudley, J.R. Wunderlich, P.F. Robbins et al., *Cancer regression and autoimmunity in patients after clonal repopulation with anti-tumor lymphocytes*, Science, 298 (2002), pp. 850–854.
[10] J. Hale, *Asymptotic Behavior of Dissipative Systems*, Amer. Math. Soc., Providence, RI, 1988.
[11] E. Hooijberg, J.J. Ruizendaal, P.J. Snijders, E.W.M. Kueter, J.M.M. Walboomers, and H. Spits, *Immortalization of human CD8$^+$ T cell clones by ectopic expression of telomerase reverse transcriptase*, J. Immunol., 165 (2000), pp. 4239–4245.
[12] N.N. Hunder, H. Wallen, J. Cao, D.W. Hendricks, J.Z. Reilly, and R. Rodmyre, *Treatment of metastatic melanoma with autologous CD4$^+$ T cells against NY-ESO-1*, New Engl. J. Medicine, 358 (2008), pp. 2698–2703.
[13] C.H. June, *Principles of adoptive T cell cancer therapy*, J. Clin. Inv., 117 (2007), pp. 1204–1212.
[14] D. Kirschner and J.C. Panetta, *Modelling immunotherapy of the tumor-immune interaction*, J. Math. Biol., 37 (1998), pp. 235–252.
[15] P. Kleihues, D.N. Louis, and B.W. Scheithauer, *Improving alloreactive CTL immunotherapy for malignant gliomas using a simulation model of their interactive dynamics*, Cancer Immunol. Immunother., 61 (2002), pp. 215–225.
[16] Y. Kogan, U. Forys, N. Kronik, O. Shukron, and Z. Agur, in preparation.
[17] N. Kronik, Y. Kogan, V. Vainstein, and Z. Agur, *Improving alloreactive CTL immunotherapy for malignant gliomas using a simulation model of their interactive dynamics*, Cancer Immunol. Immunother., 57 (2008), pp. 425–439.
[18] Carol Kruse, *personal communication*, 2007.
[19] C.A. Kruse, L. Cepeda, B. Owens, S.D. Johnson, J. Stears, and K.O. Lillehei, *Treatment of recurrent glioma with intracavitary alloreactive cytotoxic T lymphocytes and Interleukin-2*, Cancer Immunol. Immunother., 45 (1997), pp. 77–87.
[20] C.A. Kruse and D. Rubinstein, *Cytotoxic T-lymphcytes reactive to patient major histocompatibility complex proteins for therapy of brain tumors*, in Brain Tumor Immunotherapy, L.M. Liau, D.P. Becker, T.F. Cloughesy, and D.D. Bigner, eds., Humana Press, Totowa, NJ, 2001, pp. 149–170.
[21] V.A. Kuznetzov, I.A. Makalkin, M.A. Taylor, and A.S. Perelson, *Nonlinear dynamics of immunologenic tumors: Parameters estimation and global bifurcation analysis*, Bull. Math. Biol., 56 (1994), pp. 295–321.
[22] L.M. Liau, R.M. Prins, S.M. Kiertscher, S.K. Odesa, T.J. Kremen, A.J. Giovannone, J. Lin, D.J. Chute, P.S. Mischel, T.F. Cloughesy, and M.D. Roth, *Dendritic cell vaccination in glioblastoma patients induces systemic and intracranial T-cell responses modulated by the local central nervous system tumor microenvironment*, Clin. Cancer Res., 11 (2005), pp. 5515–5525.
[23] R.A. Morgan, M.E. Dudley, J.R. Wunderlich, M.S. Hughes, J.C. Yang, R.M. Sherry, R.E. Royal, S.L. Topalian, U.S. Kammula, N.P. Restifo, Z. Zheng, A. Nahvi, C.R. de Vries, L.J. Rogers-Freezer, S.A. Mavroukakis, and S.A. Rosenberg, *Cancer regression in patients after transfer of genetically engineered lymphocytes*, Science, 314 (2006), pp. 126–129.
[24] N. Bellomo, M.L. Bertotti, and S. Motta, *Cancer immune system competition: Modelling and bifurcation problem*, in Cancer Modeling and Simulation, Chapman and Hall/CRC, London, 2003.
[25] M.W.J. Schreurs, J.A. Hermsen, R.I. Klein Geltnik, K. Scholten, A.A.T.P. Brink, E.W.M. Kueter, M. Tijssen, C.J. Meijer, B. Ylstra, G.A. Meijer, and E. Hooijberg, *Genomic stability and functional activity may be lost in telomerase-transduced human CD8$^+$ T lymphocytes*, Blood, 106 (2005), pp. 2663–2670.
[26] M.W.J. Schreurs, K.B.J. Scholten, E.W.M. Kueter, J.J. Ruizendaal, C.J.L.M. Meijer, and E. Hooijberg, *In vitro generation and life span extension of human papillomavirus type 16-specific, healthy donor-derived CTL clones*, J. Immunol., 171 (2003), pp. 2912–2921.

[27] H.H. Steiner, M.M. Bonsanto, P. Beckhove, M. Brysch, K. Geletneky, R. Ahmadi, R. Schuele-Freyer, P. Kremer, G. Ranaie, D. Matejic, H. Bauer, M. Kiessling, S. Kunze, V. Schirrmacher, and C. Herold-Mende, *Antitumor vaccination of patients with glioblastoma multiforme: A pilot study to assess feasibility, safety, and clinical benefit*, J. Clin. Oncol., 22 (2004), pp. 4272–4281.

[28] G.P. Taylor, S.E. Hall, S. Navarrete, C.A. Michie, R. Davis, A.D. Witkover, M. Rossor, M.A. Nowak, P. Rudge, E. Matutes, C.R. Bangham, and J.N. Weber, *Effect of Lamivudine on human T-cell leukemia virus type* 1 *(HTLV-*1*) DNA copy number, T-cell phenotype, and antitax cytotoxic T-cell frequency in patients with HTLV-*1*-associated myelopathy*, J. Virol., 73 (1999), pp. 10289–10295.

[29] N.C. Verra, A. Jorritsma, K. Weijer, J.J. Ruizendaal, A. Voordouw, P. Weder, E. Hooijberg, T.N. Schumacher, J.B. Haanen, H. Spits, and R.M. Luiten, *Human telomerase reverse transcriptase-transduced human cytotoxic T cells suppress the growth of human melanoma in immunodificient mice*, Cancer Res., 64 (2004), pp. 2153–2161.

[30] W.D. Wick, O.O. Yang, L. Corey, and S.G. Self, *How many human immunodeficiency virus type* 1*-infected target cells can a cytotoxic T-lymphocyte kill?*, J. Virol., 79 (2005), pp. 13579–13586.

[31] M. Wölfl, *private communication*, 2007.